

Thin Profile Wideband Printed Monopole Antenna for Slim Mobile Handsets Applications

Pradutt K. Bharti, Hari S. Singh, Gaurav K. Pandey, and Manoj K. Meshram*

Abstract—In this paper, a compact wideband planar monopole antenna suitable for slim mobile handsets applications is presented. The proposed antenna operates over LTE700/GSM800/900 (0.742 GHz–1.36 GHz), GPS L1/GSM1800/1900/UMTS/IMT2100/Wi-Fi/LTE2300/2500 (1.475 GHz–2.7 GHz), and WiMAX (3.4 GHz–3.72 GHz) based on reflection coefficient better than -6 dB. It consists of coupling strip, shorted radiating strip, and parasitic meandered lines. The wider impedance bandwidth is achieved by placing the meandered line as parasitic element on the back side of the coupling and shorted radiating elements. With this configuration, the antenna gives extremely wide impedance bandwidth which covers all the required frequency bands of the smart mobile phones. To investigate the proposed antenna, S -parameters, surface current distributions, and radiation performances are studied. To check the robustness of the proposed antenna, investigation is also carried out in the vicinity of the mobile environment. Further, specific absorption rate (SAR) is calculated on the human head and found to be below 0.535 W/kg. The simulated and measured results are found in close agreement.

1. INTRODUCTION

Recently, as the mobile market has been growing rapidly, competitive global market has been driven by extensive demand of various wireless communication systems having characteristics such as compactness, multiband, wideband, and good radiation performances. The multiband and wideband antennas can operate over different frequency bands used for increased number of applications for modern handsets. Therefore, to make simpler rather than complex and bulky system, multiband/broadband antennas can be used instead of placing multiple antennas for different applications. Hence, thin profile compact wideband internal antennas are emerging trends in the modern mobile handset industry.

To achieve the requirements, several multiband and wideband antennas for mobile handsets applications have been reported, such as inverted-F antenna (IFA) [1–3] and planar inverted-F antenna [4–12]. Although both IFA and PIFA are multiband compact antennas with quarter wavelength structure, suitable for conventional mobile handsets, they exhibit additional height in addition to the substrate thickness which gives system design complexity. When the height between the radiating strip and ground plane is reduced, the operating bandwidths of IFAs and PIFAs are generally reduced, and it is difficult to achieve the desired bands with compact structure. This limits the application of PIFAs in thin-profile modern mobile phones. Further, some of the PIFAs are studied with the bandwidth enhancement techniques [13–15]. In [13], ultra wideband PIFA with capacitive feed for penta-band folder-type mobile phone is presented in which antenna is placed at the hinge position between the main and upper ground planes for the folder-type mobile phone. A multiband handset antenna combining a PIFA and multi-slots on a ground plane was studied in [14]. Slots on the ground plane act as parasitic radiators and help to tune the ground plane resonance. Inverted L-shaped parasitic

Received 15 April 2015, Accepted 20 May 2015, Scheduled 26 May 2015

* Corresponding author: Manoj Kumar Meshram (mkmeshram.ece@iitbhu.ac.in).

The authors are with the Department of Electronics Engineering, Indian Institute of Technology (Banaras Hindu University), Varanasi 221 005, India.

element, rectangular parasitic element, and change in the width of feed plate/shorting plate are used for broadening the bandwidth [15].

All the above discussed bandwidth enhancement techniques create extra design complexities due to the non-planar structure and tuning of ground slots on the mobile circuit board. Meanwhile, the folded loop with chip element (inductor and capacitor) antennas for mobile handsets have also been studied [16–20]. The radiating structures of folded chip antennas consist of multiple layers. These layers are connected through shorting pin. The adjustment of the multiple layers inside the mobile phone is complicated because adjustment of gap between multiple layers is difficult task for antenna designer. In addition to this, to make compact geometry, antenna is loaded with chip element such as capacitor and inductor which bring the losses. Due to the chip element, the total radiated power decreases which results in decrease of radiation efficiency. On the other hand, the planar monopole antennas are one of the preferable candidates for slim mobile handsets. The planar monopole antenna is quarter wavelength resonating structure which can be easily etched during the fabrication of printed circuit board (PCB) of mobile phones.

Some of the monopole antennas are studied to obtain different wireless communication bands including next generation communication bands [21–27]. In [21], two inverted-L branches and an open stub are studied for impedance tuning to achieve the GSM900 and DCS/PCS/UMTS frequency bands. Zhang et al. [22] discussed monopole antenna, which consists of two-strip monopole and a meandered strip which covers GSM850/900 and GSM1800/1900/UMTS/LTE2300/2500 frequency bands. In [23], a quad-band compact printed monopole antenna is demonstrated for GSM900/DCS/PCS/WLAN applications. In [24], a compact multi-band planar monopole antenna is proposed for slim mobile handset applications which operate over GSM900/1800/1900/UMTS/IMT2100/WLAN/LTE2500/WiMAX frequency bands. The above reported monopole antennas in [21–23] operate over the GSM850/900 frequency band at lower frequency and cover most of the wireless communication bands at higher frequency except WiMAX. Further effort has been made for widening the lower operating band to cover LTE700 along with GSM850/900 band [25–27]. Coupled feed PIFA [25, 26] was used for widening the lower operating frequency band in addition to the higher operating frequency bands. However, these antennas utilize some height from the substrate and occupy a large area. Therefore, these are not suitable for slim mobile handsets. Also, WiMAX frequency band is still not covered in above studies. Therefore, planar monopole with compact size, multiband/wideband operation is still interesting topic for the antenna designers.

In this paper, a low profile extremely wideband printed monopole antenna is presented. The proposed antenna operates over the LTE700/GSM800/900, GPS L1/GSM1800/1900/UMTS/IMT2100/Wi-Fi/LTE2300/2500, and WiMAX frequency bands based on -6 dB reflection coefficients. The simulated and measured results are found in good agreement. The configuration of the proposed antenna consists of two strips named as coupling strip and shorted radiating strip at top of the substrate, whereas meandered parasitic strip at bottom of the substrate. The bottom meandered strip helps in widening the overall operating bands by increasing the capacitance between the main radiating strip and meandered parasitic strip. Due to the capacitive coupling between the top and bottom elements, capacitance comes into the picture. The proposed antenna is elaborated through S -parameters analysis including typical shape parameters, surface current distributions, and radiation performances. Further, study is carried out in the vicinity of the mobile environment and user proximity. SAR is also calculated, and the results are found within the standard limit. The antenna configuration, results and discussion are presented in the following sections.

2. ANTENNA CONFIGURATION AND DESIGN

The proposed antenna is designed on a 0.8 mm thick FR4 substrate of dielectric constant 4.4 and loss tangent 0.018. The size of the mobile circuit board is chosen as 110×50 mm². The printed antenna is deposited on the top of the mobile circuit board of footprint 15×50 mm². The front and rear views of the proposed antenna along with the fabricated prototype is shown in Figure 1(a). The radiating element is placed on the front side as well as rear side of the substrate on the no ground portion. The ground plane is also printed on the rear side of the substrate. The coupling and shorting radiating strips are placed on the front side whereas meandered line parasitic strip is placed on the rear side

of the substrate. The details of the front and rear side radiating elements are shown in Figure 1(b) and Figure 1(c), respectively. The optimized shape parameters of the proposed antenna are shown in Table 1.

Further, the design concept of the proposed antenna is illustrated with the help of Figure 2. The

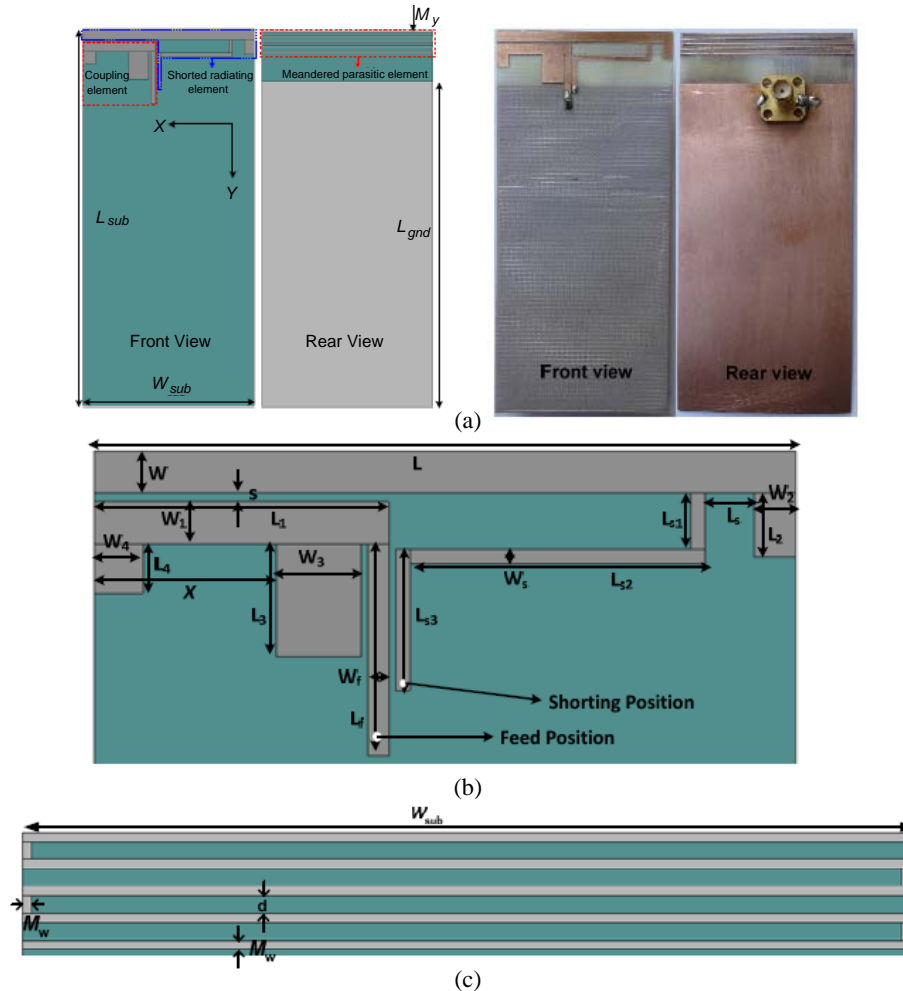


Figure 1. (a) Front and rear view of the proposed antenna. (b) Details of front side radiating element. (c) Details of rear side parasitic meandered strip.

Table 1. Optimized shape parameters of the proposed antenna.

Parameters	Value (mm)	Parameters	Value (mm)	Parameters	Value (mm)
W_{sub}	50	L_3	8	X	13
L_{sub}	110	W_3	6	W_f	1.5
L_{gnd}	95	L_4	3.5	L_f	15
L	50	W_4	3.7	d	1
W	3	L_s	3.5	W_w	0.5
L_1	21	L_{s1}	4	M_y	0
W_1	3	L_{s2}	21	Feed Position	(29.75, 19.6)
L_2	5.65	L_{s3}	10	Shorting Position	(28, 16.5)
W_2	3	s	0.6		

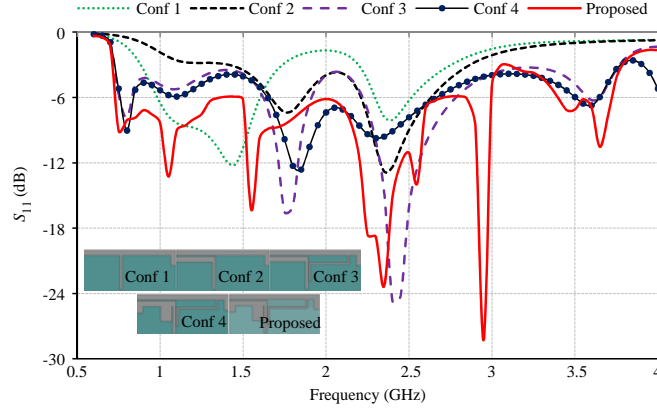


Figure 2. The variation of the reflection coefficient with frequency for different configurations during evolution.

antenna design starts with a conventional rectangular monopole antenna fed with a $50\ \Omega$ microstrip line (conf 1) which shows dual-band characteristics about 1.2 GHz and 2.4 GHz. The dual-band behaviour is observed due to the two branches of the T-shaped radiator. After that, the direct feed is replaced by coupled feed (Conf 2). The two branches of the T-shaped radiator are replaced by coupled element and driven element, which results in more matching towards higher frequency band while the lower frequency band disturbs and shifts towards higher frequency side with reduced bandwidth. After that, a shorting strip is added to the radiating strip of coupled fed monopole antenna (conf 3) which results in an additional resonating frequency band about 0.77 GHz towards lower frequency side while matching improves at higher frequency bands about 1.7 GHz and 2.4 GHz. The lower resonant frequency of the proposed antenna can be approximated as,

$$f_r = \frac{c}{\lambda_{eff}}$$

$$\lambda_{eff} \approx \frac{8 * (\text{Length of the radiating strip} + \text{Length of shorting strip})}{\epsilon_{eff}}$$

$$\epsilon_{eff} = \frac{\epsilon_r + 1}{2}$$

$$\text{Length of radiating strip} = L + L_2$$

$$\text{Length of The shorting strip} = L_{s1} + L_{s1} + L_{s1}$$

In Conf 4, two tuning stubs are added to the driven elements to tune the impedance bandwidth. Thus, the impedance matching improves significantly about 2 GHz which results in a wideband from 1.6 GHz to 2.7 GHz with respect to -6 dB reflection coefficient. Impedance matching about 0.77 GHz and 3.6 GHz improve due to these stubs. Further, a meandered line parasitic strip is placed on the rear side of the substrate below the antenna to form the proposed optimized antenna that operates in wideband from 0.73 GHz to 3 GHz along with coverage of WiMAX band from 3.3 GHz to 3.7 GHz. The parasitic element below the antenna structure can accommodate multiple resonating modes along with the main antenna structure which results in the wideband operations having multiple resonances and most of the important communication bands such as LTE700/GSM800/900 (0.742 GHz–1.36 GHz), GPSL1/GSM1800/1900/UMTS/IMT2100/Wi-Fi/LTE2300/2500 (1.475 GHz–2.7 GHz) and WiMAX (3.4 GHz–3.72 GHz).

3. SURFACE CURRENT DISTRIBUTION

The simulated surface current distributions on the proposed antenna at different frequencies (0.77 GHz, 1.8 GHz, and 3.5 GHz) are presented in Figure 3. At 0.77 GHz, the relatively strong current distributions are observed on the shorted L-strip sections. Due to the strong mutual coupling between coupling and radiating strips, the current starts flowing on shorted L-strip section. The capacitive coupling between

main radiating elements and parasitic meandered line structure (which is placed on rear side of the substrate) takes place, and due to which the current is also equally concentrated at the meandered strip at lower frequency. The current distribution at 1.8 GHz illustrates that the strong current distributions at shorting strip. This is because the resonance appears at 1.8 GHz (as shown in Figure 2). The appearance of resonance at 1.8 GHz confirms that the shorting strip is main contributing structure at this frequency. From the vector current distribution at 3.5 GHz, strong current distribution is observed at coupling elements and also at the portion of meandered parasitic which is covered with the coupling elements. The strong current distribution on the coupling strip and back side meandered parasitic is confirmed by (Figure 2) the resonance at 3.5 GHz is due to the coupling elements and end portion of the shorting strip.

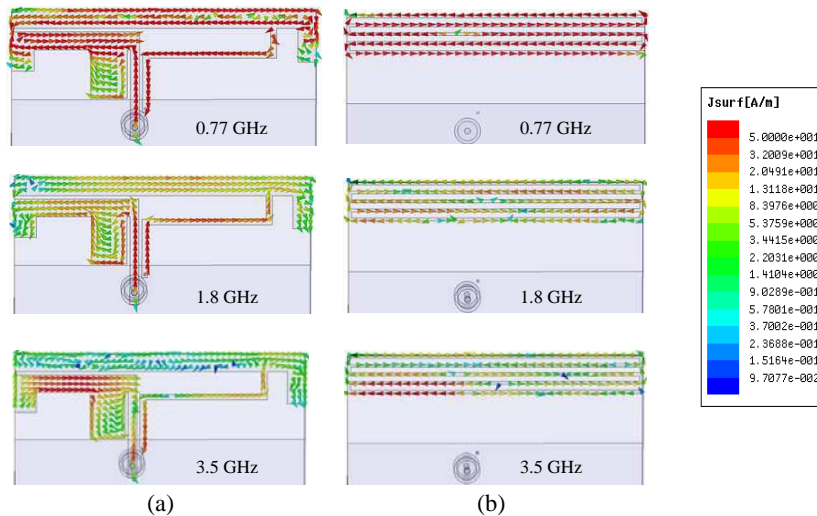


Figure 3. Vector surface current distribution at different frequencies. (a) Front view. (b) Rear view.

4. RESULTS AND DISCUSSION

All the simulations of the proposed antenna are performed originally with finite element method (FEM) based Ansoft's high frequency structure simulator (HFSS) [28] to optimize the antenna parameters for the desired operating bands. After that, the optimized antenna is fabricated using T-Tech QC5000 micro-milling machine. The simulated results of the antenna are validated with finite integration technique (FIT) based simulation software CST Microwave Studio (CST MWS) [29] and measured results. Further, CST MWS is used for SAR calculations on human head phantom.

4.1. Reflection Coefficient

The reflection coefficient variation of the proposed antenna with frequency in free space is shown in Figure 4. It is observed that the measured and simulated results are in good agreement while some discrepancies are observed which may be due to fabrication imperfection. The measured results show that the antenna operates over prerequisite 0.742 GHz–1.36 GHz, 1.475 GHz–2.7 GHz and 3.4 GHz–3.72 GHz frequency bands with -6 dB reflection coefficient.

4.2. Parametric Analysis

Further, parametric analysis of some critical dimensions/shapes of the antenna is carried out to analyze the effect of the shape parameters on the operating frequency bands using HFSS. The variation of the separation 's' between the driven and coupled elements on impedance bandwidth is shown in Figure 5(a). It is observed that impedance matching affects all over the frequency band. For $s = 0.9$ mm impedance matching is improved in about all the frequency bands with some significant mismatch about

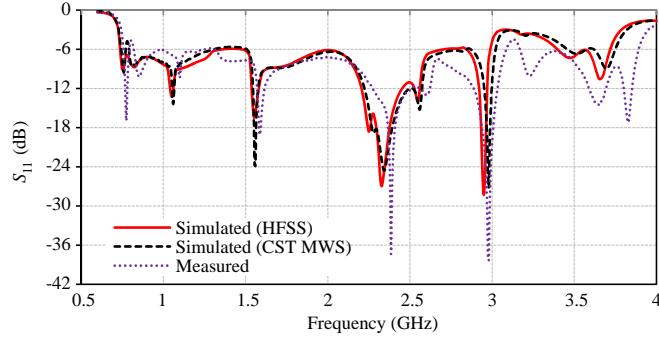


Figure 4. Simulated and measured reflection coefficient.

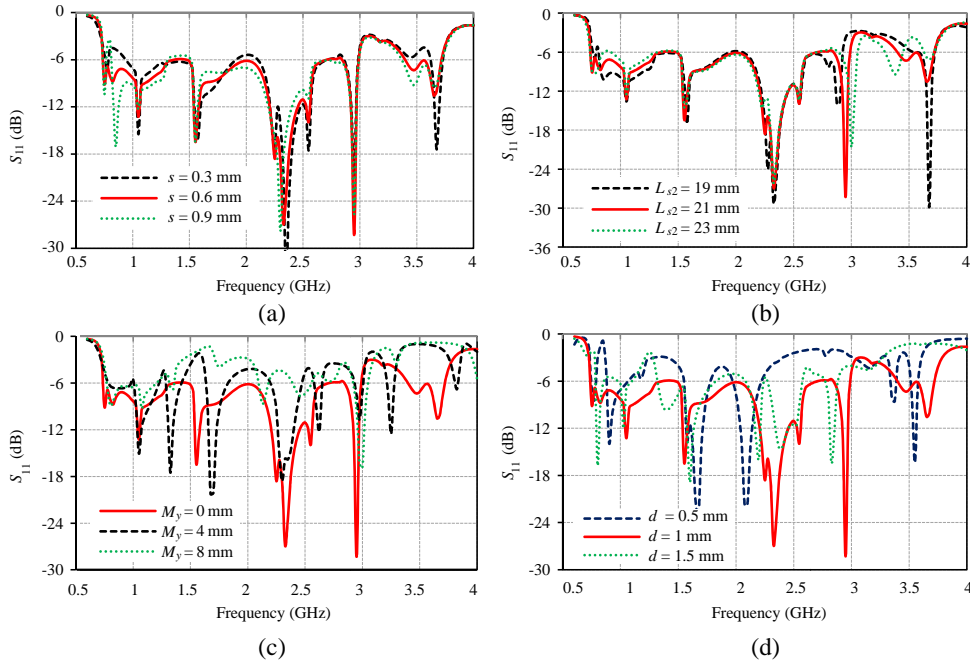


Figure 5. Variation of the reflection coefficient with shape parameters (a) s , (b) L_{s2} , (c) M_y , and (d) d .

GSM800 band whereas for $s = 0.3$ mm impedance matching gets deteriorated significantly towards lower frequency bands as well as WiMAX bands; therefore, the optimized value is taken as 0.6 mm. The effect of variation of the position of shorting strip connection position at the coupled strip L_{s2} on impedance bandwidth is shown in Figure 5(b). It is observed that impedance matching significantly affects GSM800 band and WiMAX bands due to L_{s2} variation. With decrease of the L_{s2} matching improves towards lower frequency side while deteriorating at higher frequency side. Further, the position of the meandered parasitic element position (M_y) is carried out, and it plays significant role on the impedance matching shown in Figure 5(c). It is observed that when the meandered line shifts from the top position, impedance matching gets disturbed while at the extreme top position, wideband characteristics are observed. When the gap between the meandered line horizontal arm increases, the matching towards higher frequency decreases with some improvements towards lower frequency side, for the $d = 1$ mm wide impedance matching is observed in Figure 5(d).

4.3. Radiation Performances

The measured and simulated radiation patterns of the proposed antenna at different frequencies (0.9 GHz, 1.8 GHz, 2.45 GHz, and 3.5 GHz) in xz -plane and yz -plane are plotted in Figure 6(a). The

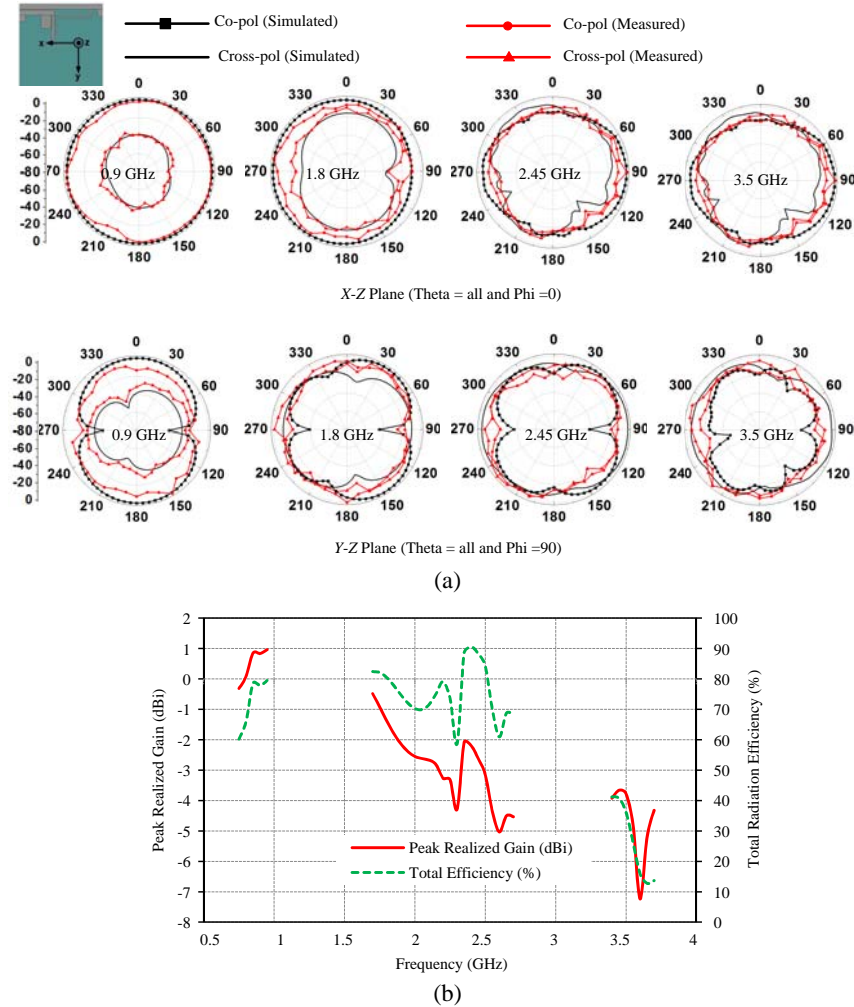


Figure 6. (a) Simulated and measured radiation patterns. (b) Variation of peak realized gain and total efficiency with frequency.

measured and simulated radiation patterns are observed in agreement. It is observed that in xz -plane the co-polar patterns show quasi omnidirectional nature at all the frequency points. At low frequency (0.9 GHz) cross-polar level is very low while as the frequency increases the cross-polar level rises and becomes comparable to the co-polar level. In yz -plane, dumbbell shape co-polar patterns are observed at all the frequencies points, and the cross-polar patterns show the same behaviour as in xz -plane. The total efficiency is calculated by considering the mismatch losses which is shown in Figure 6(b). It is observed that the variations of total efficiency lie between 60%–81% at lower operating bands, i.e., LTE700/GSM800/900 (0.742 GHz–1.36 GHz) whereas 54%–90% at the higher frequency bands, i.e., GPS L1/GSM1800/1900/UMTS/IMT2100/Wi-fi/LTE2300/2500 (1.475 GHz–2.7 GHz). At the WiMAX (3.4 GHz–3.72 GHz), the variations of total efficiency are between 13%–41%. The variations of the peak realized gain are also shown in Figure 6(b). It is observed that peak realized gain lies between -0.3 dBi and $+1$ dBi at lower operating bands whereas at higher frequency bands it lies between 0 dBi and -4 dBi.

5. ANTENNA CHARACTERIZATION IN MOBILE ENVIRONMENT

The proposed antenna is also investigated in the vicinity of the mobile environment. Mobile environment is made up with the plastic housing ($60 \times 120 \times 143 \text{ mm}^3$), LCD display ($48 \times 80 \times 2 \text{ mm}^3$) and the battery ($335 \times 505 \times 4 \text{ mm}^3$). A setup is designed in Ansoft’s HFSS as shown in Figure 7(a). The battery

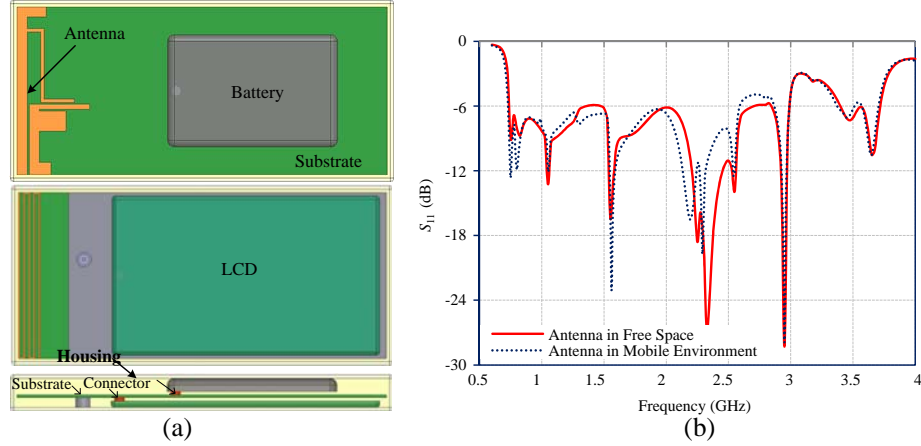


Figure 7. (a) Antenna in mobile environment. (b) Effect of mobile environment on S -parameters.

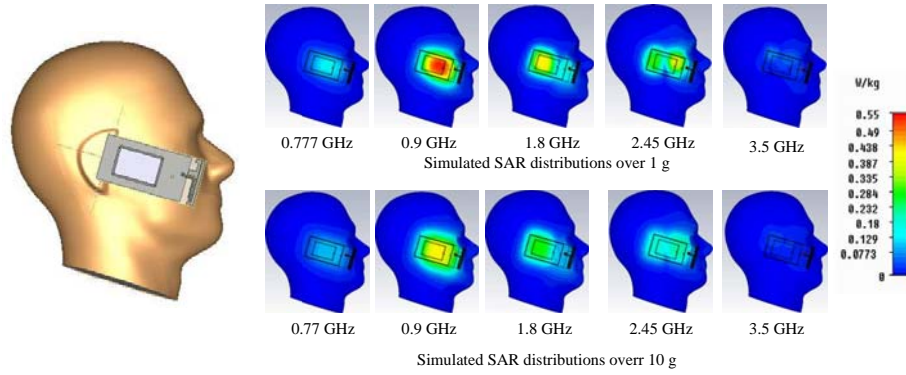


Figure 8. SAR simulation setup and SAR distribution on SAM head phantom.

and LCD are assumed a PEC (perfect electric conductor) material. The LCD is placed on the rear side of the substrate (towards ground plane) and the battery placed on the front side of the substrate where antenna is fabricated, and the components have air-gap of 1 mm from surface of the substrate. Both the components are connected to the board with metallic connecting pins provided at the ends of the components. Figure 7(b) shows the variation of reflection coefficient with frequency in free space and in the mobile environment. It is observed that due to the mobile environment mismatch occurs at certain frequencies, but still all the operating bands are covered. Therefore, it can be concluded that scattering environment near antennas play significant role on the antenna performance. If operating bands are not covered under such scenario, impedance tuning is required in the mobile environment.

6. EFFECT OF THE HUMAN HEAD PHANTOM

Further, SAR is calculated by placing antenna with mobile environment near human head phantom. The radiation from antenna inside the human body can be evaluated by SAR, which represents the time rate of microwave energy absorbed inside the tissues [30],

$$SAR = \frac{\sigma}{2\rho} E^2$$

where, ρ and σ are the density (S/m) and electrical conductivity (kg/m^3) of the tissue, respectively, and E is the internal induced electric field (V/m).

The simulation setup for SAR calculation is created according to the CTIA standard [30] in the CST MWS and shown in Figure 8. The SAR values of the proposed antenna are studied at different

frequencies as shown Figure 8. The human head phantom model available in CST MWS is considered in this study which consists of two layers namely fluid and shell. Fluid is confined in the shell which is the outer layer. The dielectric properties of the fluid and shell are considered from [30]. The input power for the SAR values over 1 g and 10 g head tissues with power 24 dBm for the 0.9 GHz band, and 21 dBm for the 0.77 GHz, 1.8 GHz, 2.1 GHz, and 3.5 GHz. The calculated values of SAR over 1 g and 10 g head tissues are given in Table 2. It is observed that the obtained values are well below the specified limit (< 1.6 W/kg over 1 g and < 2 W/kg over 10 g tissues). The results indicate that the proposed antenna is a promising candidate for the modern mobile phones.

Table 2. SAR values of antenna on SAM head.

Frequency (GHz)	Input Power (dBm)	SAR over 1 g (W/kg)	SAR over 10 g (W/kg)
0.77	21	0.0702	0.055
0.9	24	0.535	0.40
1.8	21	0.422	0.279
2.45	21	0.383	0.213
3.5	21	0.0725	0.03

7. CONCLUSION

A low profile extremely wideband printed monopole antenna is demonstrated successfully. The antenna is operated in different generation mobile communication bands, i.e., LTE700/GSM800/900 (0.742 GHz–1.36 GHz), GPS L1/GSM1800/1900/UMTS/IMT2100/Wi-Fi/LTE2300/2500 (1.475 GHz–2.7 GHz) and WiMAX (3.4 GHz–3.72 GHz). All the radiating elements are planar in nature which results in planar antenna. The proposed antenna consists of shorted L-shaped radiating element and matching stub loaded coupling strip. Further, meandered parasitic element is placed on the rear side of the antenna for widening the operating band at lower frequency band as well as higher frequency bands. After successful implementation of the proposed antenna, further performances are checked in the presence of mobile environment and human head phantom. The proposed slim mobile antenna shows satisfactory operation in the actual scenario. The proposed antenna is a promising candidate for smart mobile handsets based on the antenna performances such as reflection coefficient, surface current distributions, radiation performances, and SAR.

REFERENCES

1. Lee, J. and Y. Sung, "Heptaband inverted-F antenna with independent resonance control for mobile handsets applications," *IEEE Antennas and Wireless Propag. Lett.*, Vol. 13, 1267–1270, 2014.
2. Seko, M. H. and F. S. Corraera, "A novel tri-band planar inverted-F antenna for GSM/DCS/PCS operation in mobile," *Microwave Optical Technology Lett.*, Vol. 55, 821–825, 2013.
3. Chien, C.-W. and Y.-J. Chi, "Planar hexa-band inverted-F antenna for portable device applications," *IEEE Antennas and Wireless Propag. Lett.*, Vol. 8, 1099–1102, 2009.
4. Karkkainen, M. K., "Meandered multiband PIFA with coplanar parasitic patches," *IEEE Microw. Wireless Compon. Lett.*, Vol. 15, 630–632, 2005.
5. Yoon, H.-S. and S.-O. Park, "A new compact hexaband internal antenna of the planar inverted F-type for mobile handsets," *IEEE Antennas and Wireless Propag. Lett.*, Vol. 6, 336–339, 2007.
6. Rowell, C. R. and R. D. Murch, "A capacitively loaded PIFA for compact mobile telephone handsets," *IEEE Transactions Antennas Propag.*, Vol. 45, 837–842, 1997.
7. Chien, S. L., F. R. Hsiao, Y. C. Lin, and K. L. Wong, "Planar inverted-F antenna with a hollow shorting cylinder for mobile phone with an embedded camera," *Microwave Optical Technology Lett.*, Vol. 41, 418–419, 2004.

8. Montaser, A. M., "Design of multiband PIFA with low SAR value for all commercial mobile communication bands," *International Journal of RF and Microwave Computer-Aided Engg.*, Vol. 25, No. 3, 194–201, 2015, Doi: 10.1002/mmce.20849.
9. Seol, K., Y. Jang, and J. Choi, "PIFA with PIL patch having bent feed line for GSM/DCS/UMTS/WiBro applications," *Electronics Lett.*, Vol. 43, 436–437, 2007.
10. Chattha, H. T. and Y. Huang, "Low profile dual-feed planar inverted-F antenna for wireless LAN applications," *Microwave Optical Technology Lett.*, Vol. 53, 1382–1386, 2011.
11. Chang, C.-H. and K.-L. Wong, "Printed $\lambda/8$ -PIFA for Penta-band WWAN operation in the mobile phone," *IEEE Transactions Antennas Propag.*, Vol. 57, 1373–1381, 2009.
12. Wong, K.-L. and C.-H. Huang, "Compact multiband PIFA with a coupling feed for internal mobile phone antenna," *Microwave Optical Technology Lett.*, Vol. 50, 2487–2491, 2008.
13. Wu, C.-H. and K.-L. Wong, "Ultrawideband PIFA with a capacitive feed for penta-band folder-type mobile phone antenna," *IEEE Transactions Antennas Propag.*, Vol. 57, 2461–2464, 2009.
14. Cabedo, A., J. Anguera, C. Picher, M. Ribo, and C. Puente, "Multiband handsets antenna combining a PIFA, slots, and ground plane modes," *IEEE Transactions Antennas Propag.*, Vol. 57, 2526–2533, 2009.
15. Chattha, H. T., Y. Huang, M. K. Ishfaq, and S. J. Boyes, "Bandwidth enhancement techniques for planar inverted-F antenna," *IET Microwaves, Antennas, and Propag.*, Vol. 5, 1873–1879, 2011.
16. Chi, Y.-W. and K.-L. Wong, "Compact multiband folded loop chip antenna for small-size mobile phone," *IEEE Transactions Antennas Propag.*, Vol. 56, 3797–3803, 2008.
17. Wong, K.-L. and T.-W. Kang, "GSM850/900/1800/1900/UMTS printed monopole antenna for mobile phone application," *Microwave Optical Technology Lett.*, Vol. 50, 3192–3198, 2008.
18. Li, W.-Y. and K.-L. Wong, "Internal wireless wide area network clamshell mobile phone antenna with reduced ground plane effects," *Microwave Optical Technology Lett.*, Vol. 52, 922–930, 2010.
19. Wong, K.-L. and C.-T. Lee, "Wideband surface-mount chip antenna for eight-band LTE/WWAN slim mobile phone application," *Microwave Optical Technology Lett.*, Vol. 52, 2554–2560, 2010.
20. Wong, K.-L., M. -F. Tu, C.-Y. Wu, and W.-Y. Li, "On-board 7-band WWAN/LTE antenna with small size and compact integration with nearby ground plane in the mobile phone," *Microwave Optical Technology Lett.*, Vol. 52, 2847–2853, 2010.
21. Chen, J.-H., C.-J. Ho, C.-H. Wu, S.-Y. Chen, and P. Hsu, "Dual-band planar monopole antenna for multiband mobile systems," *IEEE Antennas and Wireless Propag. Lett.*, Vol. 7, 769–772, 2008.
22. Zhang, T., R. L. Li, G. P. Jin, G. Wei, and M. M. Tentzeris, "A novel multiband planar antenna for GSM/UMTS/LTE/Zigbee/RFID mobile devices," *IEEE Transactions Antennas Propag.*, Vol. 59, 4209–4214, 2011.
23. Chen, C.-C., C.-Y.-D. Sim, and F.-S. Chen, "A novel compact quad-band narrow strip-loaded printed monopole antenna," *IEEE Antennas and Wireless Propag. Lett.*, Vol. 8, 974–976, 2009.
24. Bharti, P. K., G. K. Pandey, H. S. Singh, and M. K. Meshram, "A compact multiband planar monopole antenna for slim mobile handsets applications," *Progress In Electromagnetics Research B*, Vol. 61, 31–42, 2014.
25. Chen, S.-C. and K.-L. Wong, "Wideband monopole antenna coupled with a chip-inductor-loaded shorted strip for LTE/WWAN mobile handset," *Microwave Optical Technology Lett.*, Vol. 53, 1293–1298, 2011.
26. Chen, S.-C. and K. -L. Wong, "Bandwidth enhancement of copled-fed on-board printed PIFA using bypass radiating strip for eight-band LTE/WWAN slim mobile phone," *Microwave Optical Technology Lett.*, Vol. 52, 2059–2065, 2010.
27. Zhao, G.-H., A.-G. Wang, W. Leng, B. Chen, and H. Chen, "Wideband internal antenna with coupled feeding for 4G mobile phone," *Microwave Optical Technology Lett.*, Vol. 55, 513–516, 2013.
28. Ansoft Corporation, Online Available: <http://www.ansoft.com>.
29. CST Microwave Studio, Online Available: <http://www.cst.com>.
30. "Test plan for mobile station over the air performance," CTIA Revision 3.1, Jan. 2011.